IEEE Access
Multidisciplinary | Rapid Review | Open Access Journal

Received January 29, 2019, accepted February 17, 2019, date of publication February 26, 2019, date of current version March 13, 2019.

Digital Object Identifier 10.1109/ACCESS.2019.2901710

Deep Learning-Based Channel Prediction in Realistic Vehicular Communications

JHIHOON JOO[1], MYUNG CHUL PARK[2], DONG SEOG HAN[1], (Senior Member, IEEE), AND VELJKO PEJOVIC[3]

[1]School of Electronics Engineering, Kyungpook National University, Daegu 41566, South Korea
[2]Center for Embedded Software Technology, Daegu 41566, South Korea
[3]Faculty of Computer and Information Science, University of Ljubljana, 1000 Ljubljana, Slovenia

Corresponding author: Dong Seog Han (dshan@knu.ac.kr)

This work was supported in part by the Basic Science Research Program through the National Research Foundation of Korea (NRF) through the Ministry of Education under Grant NRF-2016R1D1A3B03934420, in part by the Korea Institute for Advancement of Technology (KIAT) grant through the Korean Government (Ministry of Trade, Industry and Energy), Multichannel Telecommunications Control Unit and Associated Software) under Grant P0000535, and in part by the Slovenian Research Agency (research core funding) under Grant P2-0098.

ABSTRACT Access to reliable estimates of the wireless channel, such as the channel state information (CSI) and the received signal strength would open opportunities for timely adaptation of transmission parameters and consequently increased throughput and transmission efficiency in vehicular communications. To design the adaptive transmission schemes, it is important to understand the realistic channel properties, especially in vehicular environments where the mobility of communication devices causes rapid channel variation. However, getting CSI estimates is challenging due to the lack of support for obtaining CSI from the chipset. In this paper, we present our efforts towards enabling reliable, up-to-date channel estimates in vehicular communications. We begin by designing and conducting a measurement campaign where we collect IQ (in-phase and quadrature) samples of the IEEE 802.11p transmission and implement CSI extraction algorithms to obtain and analyze wireless channel estimates from various real-world environments. We then propose a deep learning-based channel prediction for predicting future CSI and received signal levels. The trace-based evaluation demonstrates that our prediction approach improves the future power level estimate by 15% to 25% in terms of the root-mean-square-error compared to the latest known channel properties, thus, providing a sound basis for future efforts in anticipatory vehicular communication transmission adaptation.

INDEX TERMS Channel state information, channel prediction, vehicular communications, neural networks, LSTM.

I. INTRODUCTION

Adapting wireless transmission based on the received signal properties is one of the key paradigms enabling us to achieve the communication performance of near Shannon limit. Information on the received signal to noise ratio (SNR), for example, is the basis of the whole span of transmission rate adaptation protocols [1]–[3]. Similarly, fine-grain channel state information (CSI) in orthogonal frequency division multiplex (OFDM) transmission enables sophisticated adaptation of the channel width [4].

The received signal properties, such as SNR and CSI can be estimated either through models, describing the propagation in the given environment, or through direct measurements of the desired properties. The models are often constructed for a particular environment and assume a relative stability of the setup. The measurements utilize a feedback loop between the receiver, who measures the properties, and the sender, who then uses the properties to adapt the transmission. Consequently, the measurement-based approaches, too, expect that the wireless channel does not change within the period between the two consecutive packet receptions.

However, in the vehicle-to-vehicle (V2V) scenarios the wireless environment varies rapidly. This, first, renders the constructed models unusable, as it is difficult to generalize the surroundings between vehicle nodes [5]; second, it calls for a reconsideration of measurement-based approaches, as the channel may vary significantly within the time between consecutive packets. For example, the current channel information such as SNR and CSI can be easily

The associate editor coordinating the review of this manuscript and approving it for publication was Di Zhang.

outdated due to the rapid variation of vehicular channels. In this case, the vehicle node cannot adapt its transmission parameters based on the current channel information. Furthermore, there are no CSI feedback loops to adapt in vehicular ad hoc networks. Thus in conventional vehicular communications, the only available information the vehicle can utilize to adapt the transmission parameters is the information based on the latest received frame.

To facilitate future improvements in V2V transmission understanding and adaptation in this paper we develop an approach for channel properties measurement and prediction in real-world V2V settings. To achieve our goal, we first overcome the challenge of the lack of the CSI estimation support in commodity vehicular communication network cards. We focus on IEEE 802.11p, a part of wireless access in vehicular environments (WAVE), an OFDM-based WLAN standard specially designed for vehicular communications [6]. IEEE 802.11p is comparatively mature technology in the market, which is categorized by non-HT (high throughput) amendments, compared to the latest amendments to the Wi-Fi standard such as IEEE 802.11ax [7]. Utilizing the fact that each WAVE frame contains a short training sequence (STS) and a long training sequence (LTS) in a preamble [8], we devise a measurement campaign method that uses off-the-shelf on-board units (OBUs) and a spectrum analyzer to produce CSI estimations for each received WAVE frame. Next, we conduct measurement campaigns in actual driving environments, obtaining, to the best of our knowledge, the first dataset of WAVE CSI data from real-world V2V driving scenarios. Finally, we investigate the short-term predictability of CSI and received power in the dataset, and propose a channel information prediction.

To summarize, the main contributions of this paper are:

- The design and the implementation of a process for CSI extraction, which is able to process raw IQ (in-phase and quadrature) samples containing IEEE 802.11p frames. We verify the CSI extraction tool in static over-the-air (OTA) and cable-connection lab scenarios.
- The collection of a real-world channel characteristics dataset containing WAVE communication from different V2V driving scenarios, including both line-of-sight (LOS) and non-LOS (NLOS) environments.
- The construction and evaluation of a deep learning method for subcarrier-level CSI and frame-level received signal strength indicator (RSSI) data prediction in vehicular environments.

II. RELATED WORK

For WLAN-based vehicular communications, a number of adaptive transmission approaches have been implemented and proposed to overcome the limitations and improve the performance [9]. To maximize the performance of adaptive transmissions, it is extremely important to obtain the corresponding channel properties as accurately as possible.

In fast varying channel environments such as V2V driving scenarios, the channel models may not be as effective as the ones from other static environments. In the same context, there have been many attempts to explore the V2V channels not only in general cases, but also in special cases which are not covered by general channel models [10]–[13]. To understand the dynamic vehicular channel properties, monitoring the variation of RSSI in real world measurements has been popular in research fields of V2V communication due to its simplicity [14], [15]. In most cases RSSI is available to users so it is relatively easy to collect the RSSI measurement data. However, RSSI is limited in its ability to capture channel characteristics as it merely represents aggregated received signal strength. For instance, information about subcarrier performance in an OFDM system cannot be obtained through RSSI analysis. Consequently, the performance of an adaptive transmission such as link adaptation based on RSSI can be degraded if the frequency selective fading is severe where a few subcarriers have relatively weak responses compared to others.

On the other hand, channel state information (CSI) is able to represent the channel response in both time and frequency domains, so called channel impulse response (CIR) and channel frequency response (CFR), respectively. More importantly, CSI is an actual metric of channel utilized in the receiver, calculated with specific known sequence and it is used for equalization of the channel effects. Therefore, for understanding channel characteristics the investigation of the CSI variation is far more useful than the investigation of RSSI variation.

There have been some research efforts regarding the investigation of the CSI. Halperin *et al.* [16] have released a CSI tool for IEEE 802.11n measurement and experimentation as a firmware and drivers built on the specific commercial network interface card (NIC). However, this tool is inappropriate for our purpose since it is restricted to the specific NIC with IEEE 802.11n standard. Bloessl *et al.* [17] have introduced the software defined radio (SDR) based IEEE 802.11p prototype. It contains CSI extraction functions, but still we believe that the spectrum analyzer is more accurate than the SDR when it comes to the measurement since the main objective of the spectrum analyzer is the measurement itself. Ye *et al.* [18] have shown the capability of deep learning for channel estimation and signal detection in OFDM systems. This work focuses on the channel estimation itself purely based on simulation data, while our main interest is the channel prediction with measurement data. Yang *et al.* [19] have introduced the inter-vehicle cooperative channel estimation schemes for IEEE 802.11p.

Channel prediction has been studied in the past years. Duel-Hallen [20] has analyzed fading prediction methods and evaluated their performances. This work demonstrates that auto-regression (AR) model-based linear prediction method shows the best prediction performance in fading channels, when compared to other algorithms such as sum-of-sinusoids (SOS) model-based methods and band-limited process model-based and other basis expansion algorithms. Zeng *et al.* [21] also have utilized AR model-based linear

prediction method for the channel prediction in VANETs for the scheduling of data dissemination. Zemen *et al.* [22] have demonstrated time-variant channel prediction with dynamic subspace selection in flat-fading channels. Navabi *et al.* [23] have introduced a channel prediction using neural network, which aims to predict the angle-of-departure (AoD) of dominant path in base stations for mobile communications. Potter *et al.* also have shown the channel prediction using recurrent neural networks with extended Kalman filter [24]. Nevertheless, above works are based on simulation data generated from the channel models. On the other hand, Luo *et al.* [25] have proposed CSI prediction with measured channel data using a deep learning approach. However, this work targets 5G wireless communications in static environments. There have been few works that address channel prediction in vehicular scenarios. Anderson [26] claimed that the channel prediction using neural networks is inappropriate because of the randomness of channel properties, however, it used channel data generated from the simulation with channel models. In contrast, we experiment the possibility of channel prediction using neural networks with our CSI data from the measurement. To the best of our knowledge, this is the initial attempt to predict the V2V channel with real-world measurement data using both deep learning and AR approaches.

III. VEHICULAR CHANNEL DATA COLLECTION APPROACH

Wireless chip vendors enable only limited access to received signal properties via software drivers. Knowing fine-grain channel properties, such as CSI, is crucial for sophisticated wireless transmission adaptation. Therefore, our first objective is to enable the collection of channel properties, such as CSI and SNR for WAVE-based communication in V2V settings.

We devise an approach that consists of two steps: 1) raw IQ data collection (explained in this Section) and 2) channel state extraction (explained in Section IV). We utilize two off-the-shelf WAVE OBUs and one outdoor spectrum analyzer (Fig. 1). For the experiments in outdoor V2V driving scenarios, each OBU is installed in a separate car and connected to the antenna mounted on the roof of the car. One OBU periodically sends basic IEEE 802.11p safety messages (BSMs) at a rate of 10 Hz, while the other OBU receives BSMs and saves them into a log file. At the receiver, a spectrum analyzer is additionally installed to record the IQ samples of IEEE 802.11p frame. Raw samples would quickly overfill the data storage, thus, we trigger the IQ recording only when the signal power surpasses a certain threshold (above the noise level which is set to -70 dBm in our measurement campaign) and only for the time sufficient to capture a whole WAVE frame. The complex baseband sampling rate of the spectrum analyzer is 14 mega-samples per second (MS/s).

The transmission parameters used in our measurement campaign are as follows. To configure the communication to be as robust as possible, we set the lowest data rate and the highest transmission power since the lowest data rate utilizes a modulation and coding scheme that is the least likely to be affected by noise. The data rate is set to 3 Mbps which means binary phase shift keying (BPSK) modulation with a code rate of 1/2 in 10 MHz bandwidth. The center frequency for BSM transmission is 5.86 GHz. A transmission power is assigned to 23 dBm.

FIGURE 1. Measurement campaign for channel measurements in vehicular environments. Each vehicle is equipped with off-the-shelf OBU and the antenna mounted on the roof of the car. A signal power-triggered spectrum analyzer is installed at the receiving end.

IV. CHANNEL PROPERTIES EXTRACTION FROM IQ DATA

Once the IQ samples for the measurement are collected from the spectrum analyzer, signal processing algorithms are applied to extract CSI.

A. STRUCTURE OF IEEE 802.11P FRAME

Traces collected by our measurement approach (Section III) contain IEEE 802.11p frames. The structure of an IEEE 802.11p frame is described in Fig. 2. The frame is composed of three fields: a preamble, signal and data. A signal field includes the information of data rate and the length of the payload data that follows. Since our objective is to extract the channel information from the frame, our focus remains in the preamble only. The preamble consists of one known STS and one known LTS, irrespective of the transmission parameters used. STS is made of ten equal short symbols and LTS is composed of a half of a long symbol (i.e. cyclic prefix) and two consecutive long symbols. Often, wireless protocols use STS for frame detection and coarse frequency offset correction and LTS for alignment and fine frequency offset correction.

B. CSI EXTRACTION

We implement the CSI extraction algorithms by the IEEE 802.11 standard as a reference. CSI extraction algorithms include down sampling, frame detection,

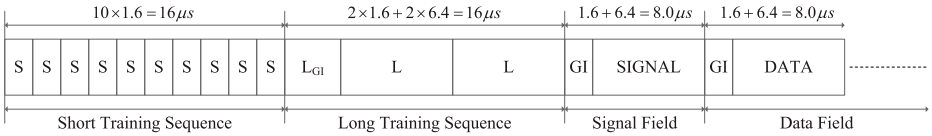

FIGURE 2. IEEE 802.11p frame structure.

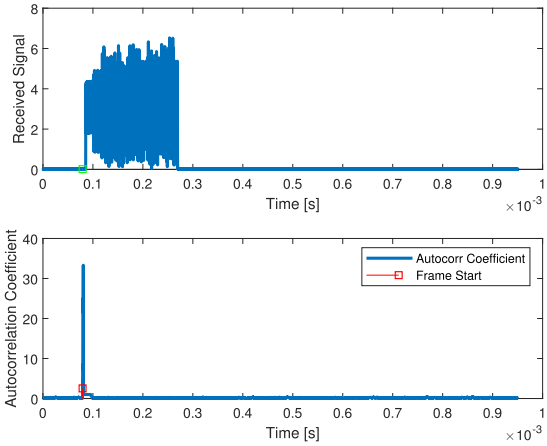

FIGURE 3. Magnitude of one example of received frame (top) and its corresponding frame detection result (bottom).

symbol alignment, frequency offset correction and training sequence extraction [17].

According to the IEEE 802.11 standard, each STS and LTS has 161 samples for 16 μs, respectively, implying 10 MS/s of sampling rate. However, raw IQ measurement data in our spectrum analyzer have 224 samples for 16 μs because of a 14 MS/s sampling rate. Thus, we need to downsample the raw IQ measurement data with the ratio of $N_{\text{tx}}/N_{\text{rx}}$, where N_{tx} and N_{rx} are the number of samples for a sequence in the transmitter and the receiver, respectively.

After downsampling of the measured IQ samples, we have to verify that the frame exists in the IQ data. We implement the frame detection algorithm by applying the autocorrelation function because STS is composed of ten repetitions of the same pattern [27]. The autocorrelation $r_{\text{ss}}[n]$ includes the complex number multiplication and is calculated as follows.

$$r_{\text{ss}}[n] = \sum_{k=0}^{N_{\text{win}}} s[n+k]\bar{s}[n+k+l_{\text{S}}] \tag{1}$$

where $s[n]$ and $\bar{s}[n]$ denote a received IQ sample and its complex conjugate, respectively. l_{S} represents the number of IQ samples for one short symbol in STS and it is 16 in IEEE 802.11p. N_{win} represents the window size for the autocorrelation and we obtain the value of N_{win} as 48 in our measurement data through experimentation with a reference [17]. Then the normalization is applied to $r_{\text{ss}}[n]$ to be independent from the input power level by dividing $r_{\text{ss}}[n]$ with the signal power. By comparing the peak value of the result and the threshold 0.5 which is predefined through experimentation with a reference [17], we can detect the frame and obtain its rough starting point in the IQ trace. Fig. 3 shows an example of conducting the frame detection algorithm. The top graph depicts the magnitude of a received frame and the bottom one depicts the result of the frame detection.

Symbol alignment is the procedure to determine the starting position of long symbols from LTS at a sample level. The positions of two long symbols are identified by the peaks from the result of cross-correlation between received IQ samples and the whole pattern in LTS. As LTS is composed of a half of pattern and two consecutive patterns, one low peak and two high peaks are detected if the IEEE 802.11p frame exists in the received IQ samples. Each peak indicates the starting point of the patterns. The cross-correlation coefficients between two high peaks are suppressed due to the sequence characteristic.

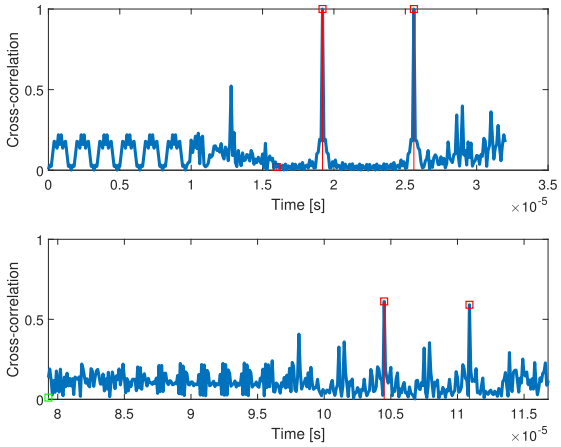

FIGURE 4. Cross-correlation results between LTS and received samples. The simulation result with perfect channel condition (top) and the result of real-world measurement (bottom).

Fig. 4 illustrates the cross-correlation results between LTS and received samples for symbol alignment. The top figure shows the simulation result with a perfect channel condition which is an identical result to the autocorrelation of LTS. The bottom figure describes the cross-correlation result for the over-the-air measurement in the laboratory. A part of the discrepancy comes from the carrier frequency offset (CFO) between the transmitter and the receiver.

To correct the CFO, we conduct both coarse and fine CFO correction [28]. Coarse frequency offset correction utilizes the repetition property of STS. As one sample in STS should be the same as the sample that is 16 samples apart within the STS, conjugate multiplication of these two samples produces

the frequency offset estimation. The calculation of the coarse frequency offset utilizes the last five short symbols of STS and is given by

$$\Delta f_{\mathrm{STS}} = \frac{1}{l_{\mathrm{S}}} angle \left(\sum_{n=0}^{5l_{\mathrm{S}}-1} \bar{s}[n] s[n + l_{\mathrm{S}}] \right) \tag{2}$$

where *angle*() denotes the phase angle in radian. Therefore, coarse frequency offset for LTS is compensated by

$$s[m] \leftarrow s[m] e^{-jm\Delta f_{\mathrm{STS}}} \tag{3}$$

where $m = 0, 1, ..., 127$ since LTS is composed of 128 samples. After coarse CFO correction, fine frequency offset is obtained in a similar manner by

$$\Delta f_{\mathrm{LTS}} = \frac{1}{l_{\mathrm{L}}} angle \left(\sum_{n=0}^{l_{\mathrm{L}}-1} \bar{s}[m] s[m + l_{\mathrm{L}}] \right) \tag{4}$$

$$s[m] \leftarrow s[m] e^{-jm\Delta f_{\mathrm{LTS}}} \tag{5}$$

where l_{L} represents the number of samples for one long symbol and in our case it is 64.

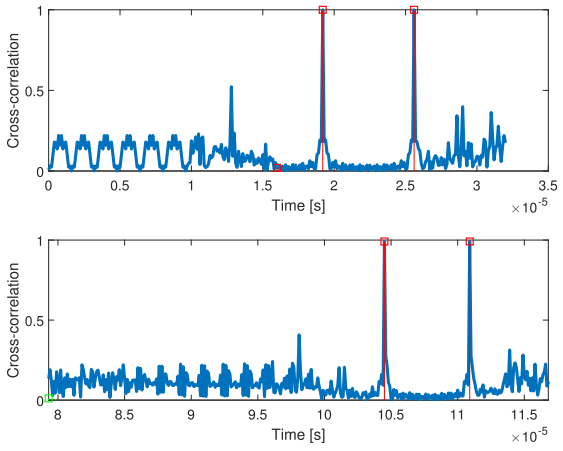

FIGURE 5. Cross-correlation results between LTS and received samples after the frequency offset correction. The simulation result with perfect channel condition (top) and the result of real-world measurement (bottom).

Fig. 5 describes the result of a symbol alignment after the frequency offset correction. The result shows that the noise effects are suppressed in LTS compared to the symbol alignment result without the frequency offset correction in Fig. 4.

We now have sufficient data to extract the CSI. From the symbol alignment, starting points of LTS patterns are determined by two peaks. Since IEEE 802.11p utilizes the 64-point fast Fourier transform (FFT), we apply the 64-point FFT to the 64 samples from first peak and the 64 samples from second peak, respectively, which yields a pattern of LTS affected by the channel. Then in the frequency domain, two CFRs from two long symbols are averaged and we employ the minimum mean square error (MMSE) algorithm to estimate channel [29]. To calculate the CSI with MMSE channel estimation, we first utilize least square (LS) estimator

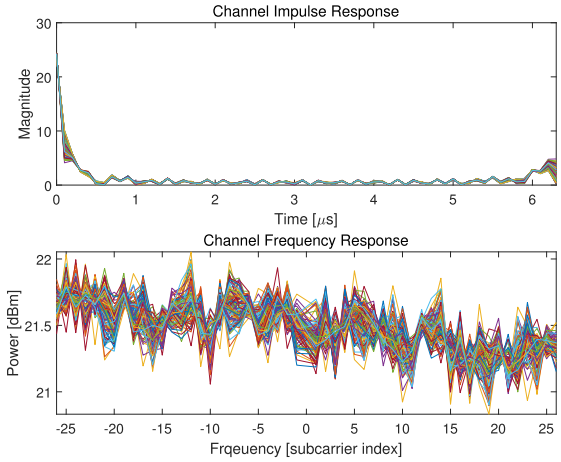

FIGURE 6. CSI extraction results from the measurement conducted on cable connection between the signal generator and the spectrum analyzer. The CIRs (top) and the CFRs (bottom) acquired from the channel estimation in the frequency domain.

which minimizes $(Y - XH)^{\mathrm{H}} (Y - XH)$ where Y denotes the averaged CFR, X is the long symbol in the frequency domain and H is the CSI. H operator means the conjugate transpose. The LS estimator of H is given by

$$\widehat{H}_{\mathrm{LS}} = X^{-1} Y \tag{6}$$

Then the MMSE estimator of H is as follows.

$$\widehat{H}_{\mathrm{MMSE}} = R_{HH} \left\{ R_{HH} + \sigma^2 \left(XX^{\mathrm{H}} \right)^{-1} \right\}^{-1} \widehat{H}_{\mathrm{LS}} \tag{7}$$

where R_{HH} can be calculated by

$$R_{HH} = E\left\{ HH^{\mathrm{H}} \right\} = E\left\{ (Fh)\,(Fh)^{\mathrm{H}} \right\} = F R_{hh} F^{\mathrm{H}} \tag{8}$$

where E means the expectation and F is a discrete Fourier transform (DFT) matrix.

V. VEHICULAR CHANNEL MEASUREMENT IN REAL-WORLD ENVIRONMENTS

We conduct measurements in different environments. First, for validation and reference purposes, we perform cable-connected measurements. The second measurement is over-the-air (OTA) measurement in the laboratory to verify the functionalities of our measurement campaign. The third one is conducted in an outdoor campus environment with two realistically moving vehicles in order to collect the data and investigate channel variation in a V2V communication setting.

A. WIRED TESTING WITH CABLE CONNECTION

To investigate our CSI extraction algorithms and identify possible distortions that the spectrum analyzer may induce, we eliminate the wireless channel effects by connecting a cable between the transmitter and the receiver. Controlled by the power-level trigger, the spectrum analyzer records 104 frames, all of which are correctly decoded by our CSI extraction module.

CSI extraction results from the measurement conducted on the cable connection are shown in Fig. 6. We show each of the frame's CSI overlapped in the same graph. As expected, the CIRs from the measurement indicated one strong signal path and the CFRs are practically flat over all subcarriers indicating little frequency selectivity. A small peak is also observed at the end of the CIRs due to the following repetitive long symbol in LTS. A received power is around 22 dBm indicating an almost 1 dB loss, as the transmission power in our measurement campaign is set to 23 dBm.

B. WIRELESS TESTING IN THE LABORATORY

To further validate our measurement approach, we also conduct the measurement in the laboratory. In this measurement, 74 frames are detected and recorded by the spectrum analyzer, while also being correctly decoded by our CSI extraction tool.

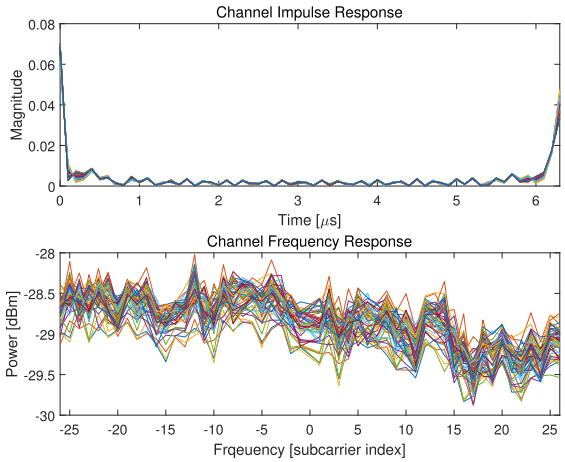

FIGURE 7. CSI extraction results from the measurement conducted in the laboratory. The CIRs (top) and the CFRs (bottom) acquired from the channel estimation in the frequency domain.

Fig. 7 describes the CSI extraction results with both CIR in time domain and CFR in the frequency domain. CSI patterns in the laboratory are similar to those in the cable-connected measurement except the received power level. The signal loss in this experiment is around 50 dB, considering the transmission power of 23 dBm and received power of −28 dBm. Flat fading is observed in the CFRs as well. The extracted CSI results are almost identical for all frames, which is expected having in mind that the environment is static.

C. CAMPUS VEHICLE-TO-VEHICLE SCENARIO

After the validation of our measurement campaign and CSI extraction tool, we extend the experiment to the campus V2V scenario. One vehicle acts as a transmitter with OBU and the other vehicle equipped with both the OBU for monitoring the packet receptions and the spectrum analyzer for recording IQ samples of the IEEE 802.11p frames. Two vehicles drive in the campus of Kyungpook National University so there are a variety of propagation environments due to the surrounding buildings, parking lots, etc. Fig. 8 shows the campus driving V2V scenario.

FIGURE 8. Snapshots taken in the receiver vehicle during the experiments in campus driving V2V scenario. Yellow circle marks the transmitter vehicle.

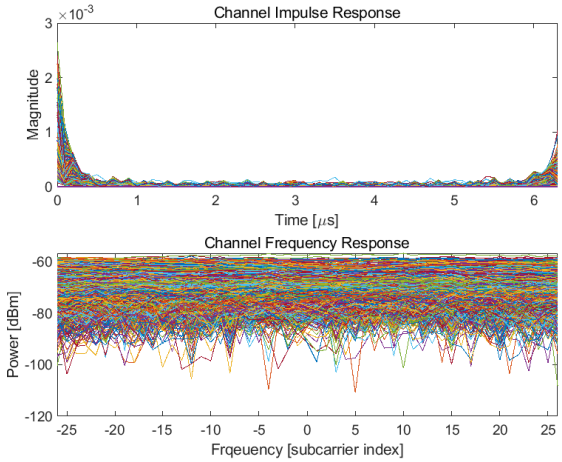

FIGURE 9. CSI extraction results from the measurement conducted in campus driving V2V scenario. The CIRs (top) and the CFRs (bottom) acquired from the channel estimation in the frequency domain.

Fig. 9 represents the CSI extraction results from the measurement conducted in campus driving V2V scenario. Each CSI is accumulated in the graph. In this measurement, 3,165 frames are detected and recorded at the spectrum analyzer, but 1,886 frames are correctly decoded by our CSI extraction module. We consider that one of the main reasons for these decoding failures is dynamic propagation environment experienced in our measurements i.e., NLOS and multipath induced by surrounding obstacles.

CSI patterns in the campus V2V scenario remain almost same to those in cable-connected and laboratory measurements. However, the CFRs vary dramatically compared to previous two static experiments due to the dynamic environment in the campus V2V scenario. Fig. 10 shows the CSI variation of the campus V2V scenario in time with a three dimensional representation. We observe both an overall received power change (e.g. higher overall level of frames

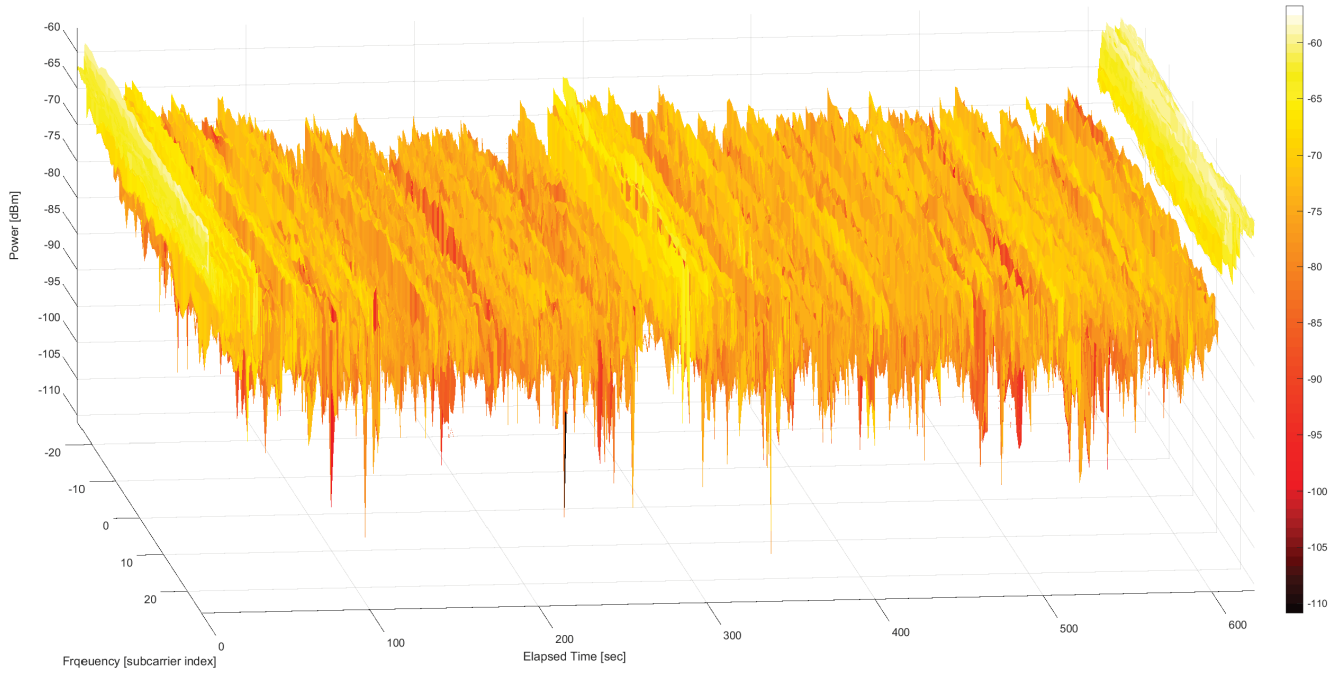

FIGURE 10. CSI extraction results from the measurement conducted in campus driving V2V scenario.

received in the beginning, at the end, and around 300 seconds into the drive), as well as frequency selective fading in individual frames. Since the experiment in the campus V2V scenario has diverse environments and numerous collected frames, the CFR analysis in time domain is able to help understanding the channel characteristics.

D. DISCUSSION

The CIRs extracted in previous three experiments exhibit a similar form although we expected to observe multipath in campus V2V driving scenario due to the surrounding obstacles. We hypothesize that the reason lies in the temporal resolution of our channel sounding approach, which is limited by the IEEE 802.11p frame structure. Paschalidis *et al.* [11] report that the RMS delay spread of multipath for campus V2V scenario is measured from minimum 0 ns to maximum 100 ns. An IEEE 802.11p frame, on the other hand, has 64 samples in 6.4 μs, leading to a 100 ns minimum resolution, rendering it unsuitable for short-distance multipath inference. For more sophisticated multipath analysis, a high-resolution channel sounder should be used. Nevertheless, our goal is to investigate channel properties extraction and prediction in a practical setting that utilizes commodity WAVE communication equipment, thus we continue our analysis while acknowledging the above limitations.

VI. EXPERIMENTAL RESULTS OF CHANNEL PREDICTION

Up-to-date knowledge of channel properties can greatly enhance the wireless communication by allowing sophisticated rate adaptation and resource allocation. Often, the adaptation is performed at the transmitter based on the last measured properties piggybacked from the receiver. However, in a dynamic environment, such as those observed in vehicular communications, the piggybacked information may already be stale by the time it reaches the sender. Therefore, in this section we explore the opportunities for *predicting* channel properties in a vehicular network setting.

We base our prediction method on the long short-term memory (LSTM) network. LSTM network is a type of a recurrent neural networks (RNN) well known for its time series prediction capabilities, and while mostly used in other domains, such as financial predictions [30], LSTM network has recently gained attraction among wireless researchers as well [31]. LSTM network is able to overcome the vanishing gradient problem which is the main issue for the conventional RNN. The structure of LSTM unit is made by adding the cell state with a forget gate layer, input gate layer and output gate layer to a hidden state of the RNN unit. Input gate i controls level of cell state update. Forget gate f controls level of cell state reset. Cell candidate g adds information to cell state and output gate o controls level of cell state added to hidden state. Each component has the input weights W, the recurrent weights R and the bias b and calculated as follows.

$$\begin{aligned} i_t &= \sigma_g \left(W_i x_t + R_i h_{t-1} + b_i\right) \\ f_t &= \sigma_g \left(W_f x_t + R_f h_{t-1} + b_f\right) \\ g_t &= \sigma_c \left(W_g x_t + R_g h_{t-1} + b_g\right) \\ o_t &= \sigma_g \left(W_o x_t + R_o h_{t-1} + b_o\right) \end{aligned} \tag{9}$$

where σ_g denotes the state activation function which is the hyperbolic tangent function and σ_c is the gate activation

function which is the sigmoid function. Therefore, the cell state c_t and the hidden state h_t at time t is given by

$$\begin{aligned} c_t &= f_t \odot c_{t-1} + i_t \odot g_t \\ h_t &= o_t \odot \sigma_c(c_t) \end{aligned} \tag{10}$$

where $\odot$ denotes the Hadamard product which takes two same-dimensional matrices and generates another matrix where each element i, j is the product of elements i, j of the original two matrices.

The neural network we utilize consists of four types of layers: a sequence input layer with one dimension, a variable number of LSTM layers with a variable number of hidden units, a fully connected layer, and a regression output layer. Data are standardized before the input layer. For the optimization algorithm, Adam [32] is applied with a maximum epoch of 250, a gradient threshold of 1, an initial learn rate of 0.005 and a learn rate drop period of 125 by the factor of 0.2.

In the rest of the paper we employ LSTM models for channel prediction and compare their performance to the baseline determined by the last observed (non-predicted) channel property value.

A. CHANNEL PREDICTION IN CAMPUS V2V SCENARIO: A SUBCARRIER LEVEL

As described in Section V-C, we have 1,886 frames-by-52 subcarriers of CSI data from the decoded frames. We first examine the ability of the LSTM network to predict a single carrier's SNR variation using a single LSTM layer (we use -26^{th} subcarrier). In Fig. 11 we show the variation of CSI of the subcarrier obtained in a real-world V2V campus drive scenario. We use the first 60% of the CSI data, which is the -26^{th} subcarrier SNR values in the channel estimation results, as a training dataset and the remaining 40% of CSI as a test dataset for the prediction. The network state keeps

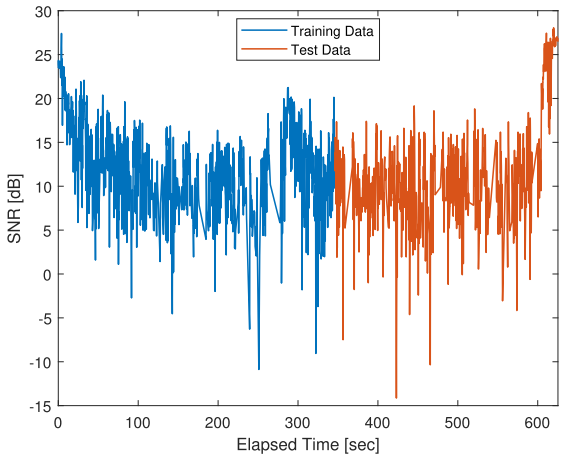

FIGURE 11. SNR variation of -26^{th} subcarrier calculated from the CSI extraction in IQ samples measured in the campus V2V scenario. First 60% of the data (blue line) are used for training and remaining 40% of the data (orange line) are used for testing.

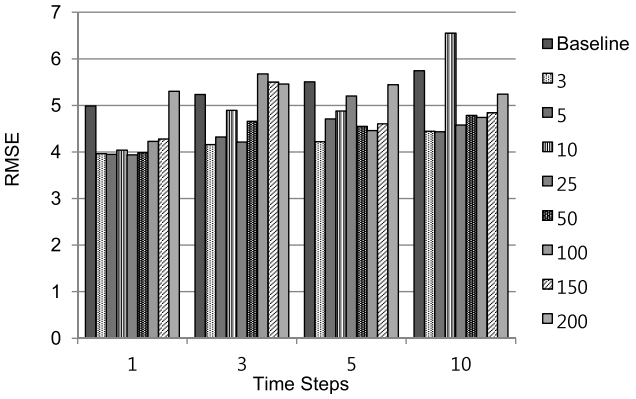

FIGURE 12. RMSE calculated between the channel prediction results and the actual CSI values in the subcarrier level campus V2V scenario. Legends describe the number of hidden units for a single LSTM layer in our experiments. Baseline represents the results utilizing the latest observed channel metric without prediction.

updating with the observed CSI since the actual values of time steps between predictions are available in our environment.

Fig. 12 shows the root-mean-square error (RMSE) of the baseline method and our channel prediction approach built with a different number of hidden units in the LSTM network. We calculate the RMSE using the actual measured power level at step t_i and the predicted power level for step t_i so the unit for the RMSE in our case is dB. The time steps values in the x-axis denote the number of frames in future that the LSTM network is making a prediction for. Overall, the prediction results show reduced RMSE compared to the baseline. Interestingly, a smaller number of hidden units in the LSTM network performs better implying that the training CSI data and the test CSI data are less correlated, which might be explained by the fact that the drive does not re-visit locations. Considering the number of hidden units as 3, the reduced RMSE margins between baseline and prediction are same 20.47% for 1 time step and 3 time steps, 23.30% for 5 time steps and 22.61% for 10 time steps, with the absolute value of LSTM's RMSE remaining almost the same. The RMSE results in this experiment are uneven with the number of hidden units due to a modest amount of data, but still we observe the advantage of neural network approach for the channel prediction.

We conducted a same experiments with 5 LSTM layers for 1 time step to evaluate the impact of the number of LSTM layers. The results are as follows: RMSE of 5.2759 with 3 LSTM units, 5.3759 with 5 units, 3.8906 with 10 units, 3.9299 with 20 units, 3.9170 with 30 units, respectively. The results indicate modest improvement despite significantly increased network complexity, thus it appears that using a single LSTM layer is sufficient for our purpose.

For a reference of prediction performance using neural networks, we provide not only a baseline with no prediction, but also a prediction with linear AR using previous measurement values. Fig. 13 shows the RMSE of prediction using AR modeled by the previous observations. Our AR model utilizes

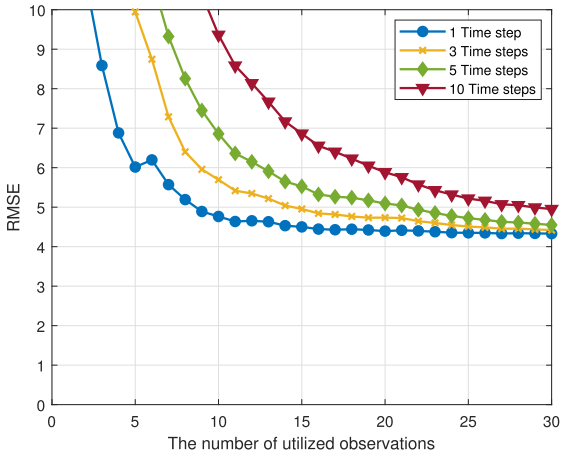

FIGURE 13. RMSE calculated between the channel prediction with AR results and the actual CSI values in the subcarrier level campus V2V scenario.

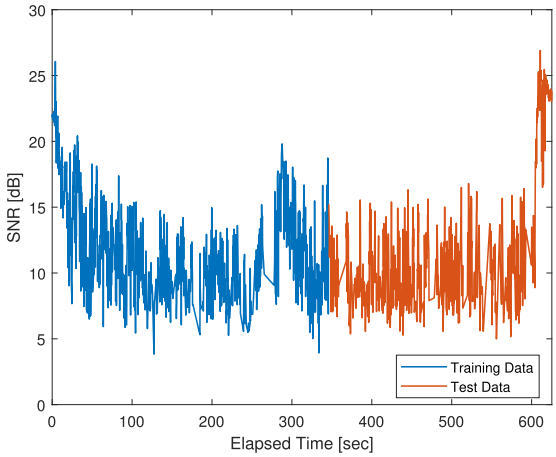

FIGURE 15. SNR variation of a decoded frame in IQ samples measured in the campus V2V scenario. First 60% of the data (blue line) are used for training and remaining 40% of the data (orange line) are used for testing.

ordinary least squares which minimizes the sum of squared errors for the fitting. The results demonstrate that channel prediction using an AR cannot achieve the performance of neural networks even in modeling with large number of previous measurements. For example with one time step, the minimum RMSE values for the AR and neural networks are 4.2053 and 3.9364, respectively.

To compare the performance of channel prediction methods, we demonstrate the best results from a deep learning and an AR in Fig. 14. In the subcarrier level campus V2V scenario, two channel prediction methods outperform the baseline but the difference between two methods is small. A deep learning shows better performance for the time step of 1 while an AR shows better performance for the time step of 10.

B. CHANNEL PREDICTION IN CAMPUS V2V SCENARIO: A FRAME LEVEL

A subcarrier-level SNR variation is highly fluctuating compared to a frame-level received power variation. A frame-level channel prediction is also useful as a subcarrier-level channel prediction for the applications such as power allocation and power adaptation, etc. With IQ samples measured in campus V2V scenario, We are able to analyze in not only the subcarrier level but also the frame level. The frame level power variation in campus V2V scenario is calculated and illustrated in Fig. 15. Similarly with the subcarrier level analysis, We use the first 60% of the CSI data as a training dataset and the remaining 40% of CSI as a test dataset for the prediction.

Fig. 16 shows the RMSE of the baseline method and our channel prediction approach built with a different number of hidden units in the LSTM network for frame level SNR analysis in the campus V2V scenario. Considering the number of hidden units as 5, the reduced RMSE margins between baseline and prediction are 14.32% for 1 time step, 19.02% for 3 time steps, 21.82% for 5 time steps and 24.51% for 10 time steps. Again, the results are uneven due to a

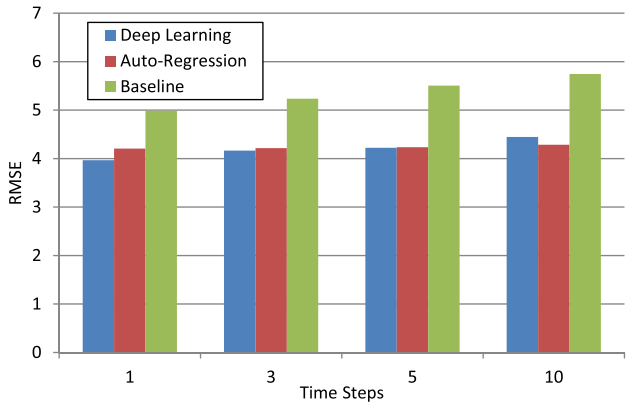

FIGURE 14. RMSE comparison between the best results from the channel prediction with a deep learning and an AR in the subcarrier level campus V2V scenario.

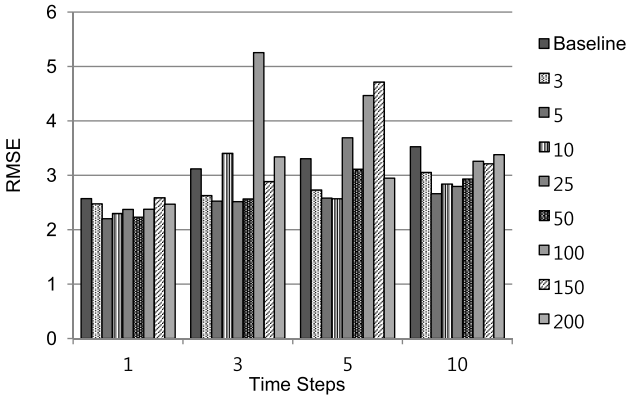

FIGURE 16. RMSE calculated between the channel prediction results and the actual SNR values in the campus V2V scenario. Legends describe the number of hidden units for a single LSTM layer in our experiments. Baseline represents the results utilizing the latest observed channel metric without prediction.

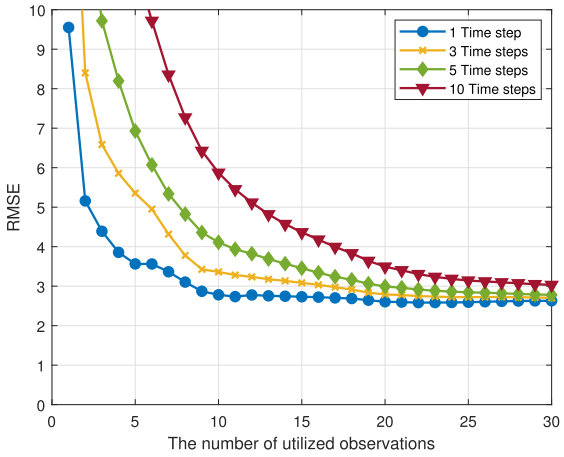

FIGURE 17. RMSE calculated between the channel prediction with AR results and the actual SNR values in the campus V2V scenario.

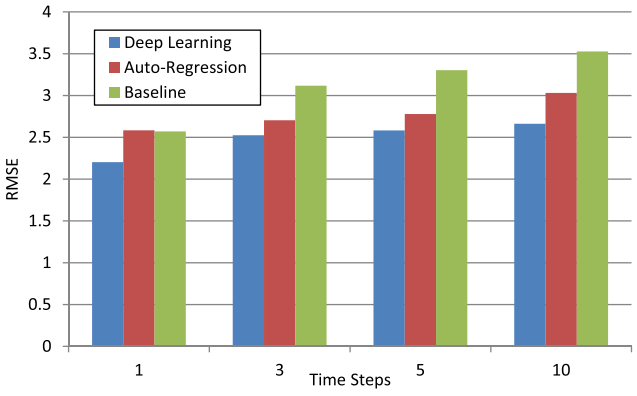

FIGURE 18. RMSE comparison between the best results from the channel prediction with a deep learning and an AR in the frame level campus V2V scenario.

modest amount of data. Compared to the previous channel prediction results in a subcarrier-level, the overall RMSEs for channel prediction are lower in frame-level. We argue that, compared to the subcarrier-level received power, the frame-level received power is already averaged over subcarriers, thus remains less sensitive to the noise leading to smoother frame-to-frame SNR measurements.

Fig. 17 shows the RMSE of prediction using AR modeled by the previous observations as a performance reference. The results also demonstrate that channel prediction using an AR has lower performance than a deep learning approach.

We also present the best results from a deep learning and an AR in Fig. 14 to compare the performance of channel prediction methods. In the frame level campus V2V scenario, a deep learning-based method shows better performance in all time steps. For time step of 1, an AR shows worse RMSE even compared to the baseline.

C. CHANNEL PREDICTION IN HIGHWAY V2V SCENARIO: A FRAME LEVEL

Besides the campus scenario, we assess our method's ability to predict channel properties in a highway V2V scenario

FIGURE 19. Snapshots taken in the receiver vehicle during the experiments in the highway V2V scenario. Yellow circle marks the transmitter vehicle.

depicted in Fig. 19. The experimental configurations are set up same as the campus scenario. The average speed of the cars in a highway is around 100 km/h and we collect the measurement data for around 1 hour. Measurement campaign for the received frame power collection is configured with off-the-shelf WAVE OBUs. The number of transmitted frames and received power information for collected frames is 120,308 and 110,372, respectively. Received power of the frame in the highway V2V scenario are shown in Fig. 20. We also apply the first 60% of received power data as a training dataset and the last 40% of received power data as a test dataset for the prediction. The network state keeps updating with the observed value as well in this experiment.

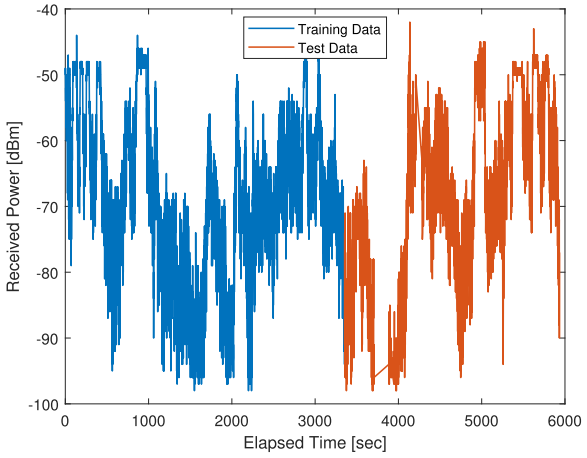

FIGURE 20. Received power variation measured in the highway V2V scenario. First 60% of the data (blue line) are used for training and remaining 40% of the data (orange line) are used for testing.

Fig. 21 shows the RMSE results of baseline and received power predictions for highway V2V data using different number of hidden units for the LSTM network. Generally, the prediction results show similar RMSE compared to the baseline similar to the results of channel prediction in the

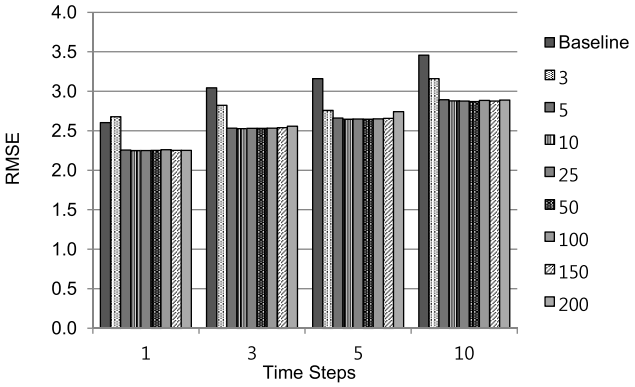

FIGURE 21. RMSE calculated between the channel prediction results and the actual CSI values in the highway V2V scenario. Legends describe the number of hidden units for a single LSTM layer in our experiments. Baseline represents the results utilizing the latest observed channel metric without prediction.

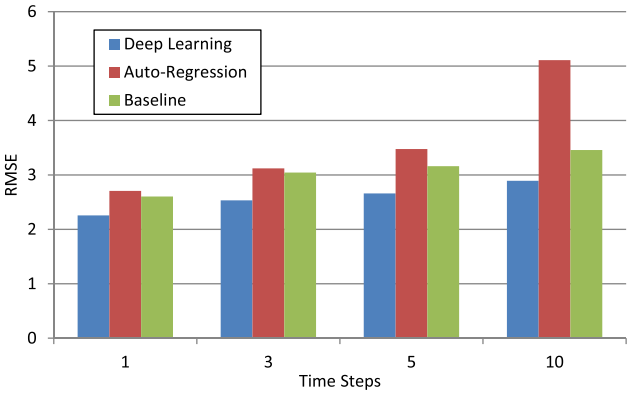

FIGURE 23. RMSE comparison between the best results from the channel prediction with a deep learning and an AR in the highway V2V scenario.

frame level campus V2V scenario. Considering the number of hidden units as 5, the reduced RMSE margins between baseline and prediction are 13.35% for 1 time step, 16.76% for 3 time steps, 15.80% for 5 time steps and 16.35% for 10 time steps. Compared to the previous channel prediction results in a subcarrier-level, the overall RMSEs for channel prediction are lower in frame-level, same as described in the campus V2V scenario. Another observation is that the number of hidden units has a minimal effect on the prediction performance when the training data are large enough. Therefore choosing a small number of hidden units is possible and should be used for the channel prediction to reduce the amount of computation needed for neural network training. In addition, the RMSE results in this experiment are relatively evenly distributed with the increasing number of hidden units compared to the results with campus V2V scenario due to a relatively modest amount of data.

We conducted a same experiments with 5 LSTM layers for 1 time step to evaluate the impact of the number of LSTM layers. The results are as follows: RMSE of 3.7138 with 3 LSTM units, 2.5709 with 5 units, 2.3104 with 10 units, 2.2679 with 20 units, 2.2496 with 30 units, respectively. We consider these results as little improvements with a huge additional complexity of the prediction system since the performance is almost same to the results using a single LSTM layer network.

Again, for a reference of prediction performance using neural networks, Fig. 22 shows the RMSE of prediction using AR modeled by the previous observations in the highway V2V scenario. The results in the highway measurements also demonstrate that channel prediction using an AR shows lower performance than the neural network.

Likewise, to compare the performance of channel prediction methods, we demonstrate the best results from a deep learning and an AR in Fig. 23. In the highway V2V scenario, a deep learning-based method shows better performance in all time steps. More interestingly, an AR shows worse performance than the baseline in all time steps in the highway measurement data.

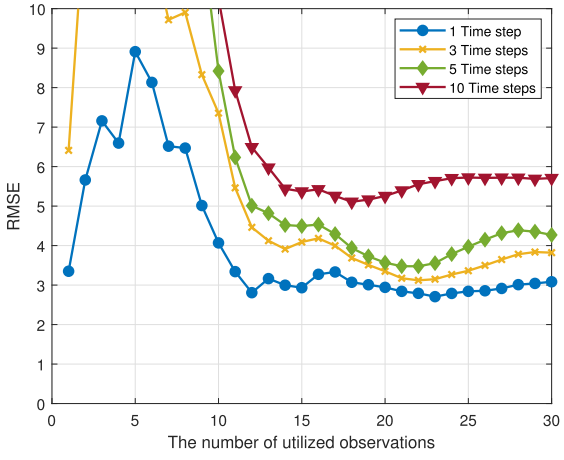

FIGURE 22. RMSE calculated between the channel prediction with AR results and the actual CSI values in the highway V2V scenario.

VII. CONCLUSIONS

In this paper, we have developed the CSI extraction tool and investigated the performance of channel prediction with a deep learning approach and an AR approach based on realistic measurement data in vehicular environments. We first have introduced our measurement campaign for recording IQ samples in the outdoor environments and the CSI extraction tool from measured IQ samples of IEEE 802.11p frame. The detailed algorithms for CSI extraction in the implementation process have been provided with equations. The results of CSI extraction in measured IQ samples have also been presented for both static and dynamic environments. Furthermore, we have exhibited the initial experimental results for channel prediction based on the real-world measured wireless channels in both subcarrier-level and frame-level. Deep learning-based channel prediction results have shown promising performance compared to the AR-based channel prediction and the latest obtained channel information.

Future work includes improving the performance of channel prediction by adding additional information to the neural networks such as the information on the surrounding environment, which may be sensed by on-vehicle sensors. Performance evaluation of adaptive transmission or resource allocation schemes will be studied accordingly.

ACKNOWLEDGMENT

The authors would like to thank Fabio Ricciato for his valuable comments that helped shape the presented research.

REFERENCES

[1] G. Holland, N. Vaidya, and P. Bahl, "A rate-adaptive MAC protocol for multi-hop wireless networks," in *Proc. 7th Annu. Int. Conf. Mobile Comput. Netw.*, Jul. 2001, pp. 236–251.

[2] B. Sadeghi, V. Kanodia, A. Sabharwal, and E. Knightly, "Opportunistic media access for multirate ad hoc networks," in *Proc. 8th Annu. Int. Conf. Mobile Comput. Netw.*, Sep. 2002, pp. 24–35.

[3] J. Camp and E. Knightly, "Modulation rate adaptation in urban and vehicular environments: cross-layer implementation and experimental evaluation," *IEEE/ACM Trans. Netw.*, vol. 18, no. 6, pp. 1949–1962, Dec. 2010.

[4] V. Pejovic and E. M. Belding, "WhiteRate: A context-aware approach to wireless rate adaptation," *IEEE Trans. Mobile Comput.*, vol. 13, no. 4, pp. 921–934, Apr. 2014.

[5] H. Ju and R. Zhang, "Throughput maximization in wireless powered communication networks," *IEEE Wireless Commun.*, vol. 13, no. 1, pp. 418–428, Jan. 2014.

[6] D. Jiang and L. Delgrossi, "IEEE 802.11p: Towards an international standard for wireless access in vehicular environments," in *Proc. IEEE Veh. Technol. Conf. (VTC Spring)*, May 2008, pp. 2036–2040.

[7] E. Khorov, A. Kiryanov, A. Lyakhov, and G. Bianchi, "A tutorial on IEEE 802.11ax high efficiency WLANs," *IEEE Commun. Surveys Tuts.*, vol. 21, no. 1, pp. 197–216, 1st Quart., 2019.

[8] Y.-C. Wu, K.-W. Yip, T.-S. Ng, and E. Serpedin, "Maximum-likelihood symbol synchronization for IEEE 802.11a WLANs in unknown frequency-selective fading channels," *IEEE Trans. Wireless Commun.*, vol. 4, no. 6, pp. 2751–2763, Nov. 2005.

[9] S. A. A. Shah, E. Ahmed, F. Xia, A. Karim, M. Shiraz, and R. M. Noor, "Adaptive beaconing approaches for vehicular ad hoc networks: A survey," *IEEE Syst. J.*, vol. 12, no. 2, pp. 1263–1277, Jun. 2018.

[10] R. Sun, D. W. Matolak, and P. Liu, "5-GHz V2V channel characteristics for parking garages," *IEEE Trans. Veh. Technol.*, vol. 66, no. 5, pp. 3538–3547, May 2017.

[11] P. Paschalidis *et al.*, "Investigation of MPC correlation and angular characteristics in the vehicular urban intersection channel using channel sounding and ray tracing," *IEEE Trans. Veh. Technol.*, vol. 65, no. 8, pp. 5874–5886, Aug. 2016.

[12] P. Liu, B. Ai, D. W. Matolak, R. Sun, and Y. Li, "5-GHz vehicle-to-vehicle channel characterization for example overpass channels," *IEEE Trans. Veh. Technol.*, vol. 65, no. 8, pp. 5862–5873, Aug. 2016.

[13] R. He *et al.*, "Vehicle-to-vehicle radio channel characterization in crossroad scenarios," *IEEE Trans. Veh. Technol.*, vol. 65, no. 8, pp. 5850–5861, Aug. 2016.

[14] M. Boban, J. Barros, and O. K. Tonguz, "Geometry-based vehicle-to-vehicle channel modeling for large-scale simulation," *IEEE Trans. Veh. Technol.*, vol. 63, no. 9, pp. 4146–4164, Nov. 2014.

[15] H.-M. Lin, H.-M. Tsai, and M. Boban, "Scooter-to-*X* communications: Antenna placement, human body shadowing, and channel modeling," *Ad Hoc Netw.*, vol. 37, pp. 87–100, Feb. 2016.

[16] D. Halperin, W. Hu, A. Sheth, and D. Wetherall, "Tool release: Gathering 802.11n traces with channel state information," *ACM SIGCOMM Comput. Commun. Rev.*, vol. 41, no. 1, p. 53, Jan. 2011.

[17] B. Bloessl, M. Segata, C. Sommer, and F. Dressler, "Performance assessment of IEEE 802.11p with an open source SDR-based prototype," *IEEE Trans. Mobile Comput.*, vol. 17, no. 5, pp. 1162–1175, May 2018.

[18] H. Ye, G. Y. Li, and B.-H. Juang, "Power of deep learning for channel estimation and signal detection in OFDM systems," *IEEE Wireless Commun. Lett.*, vol. 7, no. 1, pp. 114–117, Feb. 2018.

[19] Y. Yang, D. Fei, and S. Dang, "Inter-vehicle cooperation channel estimation for IEEE 802.11p V2I communications," *J. Commun. Netw.*, vol. 19, no. 3, pp. 227–238, Jun. 2017.

[20] A. Duel-Hallen, "Fading channel prediction for mobile radio adaptive transmission systems," *Proc. IEEE*, vol. 95, no. 12, pp. 2299–2313, Dec. 2007.

[21] F. Zeng, R. Zhang, X. Cheng, and L. Yang, "Channel prediction based scheduling for data dissemination in VANETs," *IEEE Commun. Lett.*, vol. 21, no. 6, pp. 1409–1412, Jun. 2017.

[22] T. Zemen, C. F. Mecklenbräuker, and B. H. Fleury, "Minimum-energy bandlimited time-variant channel prediction with dynamic subspace selection," in *Proc. 14th Eur. Signal Process. Conf.*, Sep. 2006, pp. 1–5.

[23] S. Navabi, C. Wang, O. Y. Bursalioglu, and H. Papadopoulos. (2018). "Predicting wireless channel features using neural networks." [Online]. Available: https://arxiv.org/abs/1802.00107

[24] C. Potter, K. Kosbar, and A. Panagos, "MIMO channel prediction using recurrent neural networks." *Int. Found. Telemetering*, 2008.

[25] C. Luo, J. Ji, Q. Wang, X. Chen, and P. Li, "Channel state information prediction for 5G wireless communications: A deep learning approach," *IEEE Trans. Netw. Sci. Eng.*, to be published. doi: 10.1109/TNSE.2018.2848960.

[26] A. J. Anderson, "Channel prediction in wireless communications," Ph.D. dissertation, Inst. Digit. Commun. School Eng., Univ. Edinburgh, Edinburgh, U.K., 2015.

[27] *IEEE Standard for Information Technology–Telecommunications and Information Exchange Between Systems Local and Metropolitan Area Networks—Specific Requirements—Part 11: Wireless LAN Medium Access Control (MAC) and Physical Layer (PHY) Specifications*, Standard IEEE Std 802.11-2016 and Revision IEEE Std 802.11-2012, 2016, pp. 1–3534.

[28] E. Sourour, H. El-Ghoroury, and D. McNeill, "Frequency offset estimation and correction in the IEEE 802.11a WLAN," in *Proc. IEEE 60th Veh. Technol. Conf. (VTC-Fall)*, vol. 7, Sep. 2004, pp. 4923–4927.

[29] J.-J. Van De Beek, O. Edfors, M. Sandell, S. K. Wilson, and P. O. Borjesson, "On channel estimation in OFDM systems," in *Proc. IEEE 45th Veh. Technol. Conf. Countdown Wireless 31st Century*, vol. 2, Jul. 1995, pp. 815–819.

[30] S. Hochreiter and J. Schmidhuber, "Long short-term memory," *Neural Comput.*, vol. 9, no. 8, pp. 1735–1780, Nov. 1997.

[31] S. Rajendran, W. Meert, D. Giustiniano, V. Lenders, and S. Pollin, "Deep learning models for wireless signal classification with distributed low-cost spectrum sensors," *IEEE Trans. Cogn. Commun. Netw.*, vol. 4, no. 3, pp. 433–445, Sep. 2018.

[32] D. P. Kingma and J. Ba. (2014). "Adam: A method for stochastic optimization." [Online]. Available: https://arxiv.org/abs/1412.6980

JHIHOON JOO received the B.S. and M.S. degrees from Kyungpook National University, Daegu, South Korea, in 2011 and 2014, respectively, where he is currently pursuing the Ph.D. degree. From 2014 to 2017, he received a Global Ph.D. Fellowship from NRF, South Korea. In 2018, he was a Visiting Scholar with the University of Ljubljana, Slovenia. His research interests include vehicular communications, wireless communications and networks, and intelligent transportation systems.

MYUNG CHUL PARK received the B.S. and M.S. degrees from Kypungpook National University, Daegu, South Korea, in 2013 and 2015, respectively. He is currently pursuing the Ph.D. degree. His current research interests include wireless communication systems and sonar signal processing.

DONG SEOG HAN (SM'07) received the B.S. degree in electronic engineering from Kyungpook National University (KNU), Daegu, South Korea, in 1987, and the M.S. and Ph.D. degrees in electrical engineering from the Korea Advanced Institute of Science and Technology, Daejon, South Korea, in 1989 and 1993, respectively. From 1987 to 1996, he was with Samsung Electronics, Co., Ltd., where he developed the transmission systems for QAM HDTV and Grand Alliance HDTV receivers. Since 1996, he has been with the School of Electronics Engineering, KNU, as a Professor. He was a courtesy Associate Professor with the Department of Electrical and Computer engineering, University of Florida, in 2004. He was the Director with the Center of Digital TV and Broadcasting, Institute for Information Technology Advancement, from 2006 to 2008. His current research interests include digital broadcasting and communication systems.

VELJKO PEJOVIC received the Ph.D. degree in computer science from the University of California at Santa Barbara, Santa Barbara, USA, in 2012, on the topic of resource-efficient wireless communication for rural areas. From 2012 to 2014, he was a Research Fellow with the University of Birmingham, U.K., in mobile computing and sensing. His work on modeling users' movement and communication behavior from mobile call records has won the 2013 Orange Data for Development Challenge, while his work on developing machine learning models of interruptibility based on sensor data resulted in the best paper nomination at the 2014 ACM UbiComp conference. He is currently an Assistant Professor with the Faculty of Computer and Information Science, University of Ljubljana, Slovenia. His current research interests include mobile sensing, particularly for human behavior inference, and wireless and resource-efficient mobile computing.